Shigella applies molecular mimicry to subvert vinculin and invade host cells

Tina Izard,[1] Guy Tran Van Nhieu,[3] and Philippe R.J. Bois[2]

[1]Cell Adhesion Laboratory, Department of Oncology, and [2]Department of Biochemistry St. Jude Children's Research Hospital, Memphis, TN 38105
[3]Unité de Pathogénie Microbienne Moléculaire, Institut Pasteur, 75724 Paris Cedex 15, France

Shigella flexneri, the causative agent of bacillary dysentery, injects invasin proteins through a type III secretion apparatus upon contacting the host cell, which triggers pathogen internalization. The invasin IpaA is essential for *S. flexneri* pathogenesis and binds to the cytoskeletal protein vinculin to facilitate host cell entry. We report that IpaA harbors two vinculin-binding sites (VBSs) within its C-terminal domain that bind to and activate vinculin in a mutually exclusive fashion. Only the highest affinity C-terminal IpaA VBS is necessary for efficient entry and cell–cell spread of *S. flexneri*, whereas the lower affinity VBS appears to contribute to vinculin recruitment at entry foci of the pathogen. Finally, the crystal structures of vinculin in complex with the VBSs of IpaA reveal the mechanism by which IpaA subverts vinculin's functions, where *S. flexneri* utilizes a remarkable level of molecular mimicry of the talin–vinculin interaction to activate vinculin. Mimicry of vinculin's interactions may therefore be a general mechanism applied by pathogens to infect the host cell.

Introduction

Shigella flexneri is the leading cause of dysentery (shigellosis) worldwide, often provoking severe colitis and diarrhea that quickly dehydrates afflicted patients, causing high morbidity and mortality, with up to 160 million cases, and 2.6 million deaths, annually (Niyogi, 2005). *S. flexneri* thrives in the human intestine, where it utilizes a type III secretion system typical of many Gram-negative pathogens to inject invasin proteins (IpaA–D) into intestinal epithelial cells (Tran Van Nhieu et al., 2000). The IpaA invasin is a 70-kD (633-residue) protein required for *S. flexneri* pathogenesis, and it facilitates entry into the host cell by binding to the N-terminal domain of vinculin (Tran Van Nhieu et al., 1997; Bourdet-Sicard et al., 1999), which is an essential protein that links the actin cytoskeleton to adhesion receptors in focal adhesions and adherens junctions (Critchley, 2004). However, the precise mechanism by which *S. flexneri* subverts vinculin functions is unknown.

The crystal structure of vinculin in its resting, inactive state revealed that the protein contains five loosely packed α-helical bundle domains clamped together through intramolecular hydrophobic interactions of vinculin's N-terminal, seven-helical bundle domain (Vh1) with its five-helical bundle tail (Vt) domain (Bakolitsa et al., 2004; Borgon et al., 2004; Izard et al., 2004). Vinculin activation requires severing of the Vh1–Vt interaction (Johnson and Craig, 1995; Gilmore and Burridge, 1996), and it was thought to be directed by the binding of phosphatidylinositol-4,5-bisphosphate (PIP_2) to the tail domain of vinculin (Gilmore and Burridge, 1996; Bakolitsa et al., 1999). However, the PIP_2 binding site is occluded in inactive vinculin (Bakolitsa et al., 2004), and vinculin mutants defective in binding to PIP_2 localize to focal adhesion complexes (Chandrasekar et al., 2005). More recently, the vinculin-binding sites (VBSs) of the adhesion proteins talin and α-actinin have been revealed as triggers that are sufficient to activate vinculin by binding to its Vh1 domain and provoking remarkable changes in its structure that displace Vt from a distance (Izard et al., 2004; Izard and Vonrhein, 2004; Bois et al., 2005, 2006; Fillingham et al., 2005).

Vinculin plays an important role in *S. flexneri* pathogenesis, as entry of the pathogen is markedly impaired in vinculin-deficient cells (Tran Van Nhieu et al., 1997). Entry of the pathogen also depends on its invasin protein IpaA, which binds to vinculin through an interaction with vinculin's Vh1 domain (Bourdet-Sicard et al., 1999). IpaA is also capable of activating the latent F-actin– and vinexin-β–binding functions of vinculin (Bourdet-Sicard et al., 1999; Chen et al., 2005). The amphipathic α-helical VBSs of talin and α-actinin are sufficient to alter the overall conformation of vinculin and to activate its ability to bind to F-actin (Bois et al., 2006). Therefore, we tested the hypotheses that *S. flexneri*'s IpaA invasin would also harbor a

Correspondence to Tina Izard: tina.izard@stjude.org

Abbreviations used in this paper: PIP_2, phosphatidylinositol-4,5-bisphosphate; SPR, surface plasmon resonance; VBS, vinculin-binding site.

The online version of this article contains supplemental material.

The Journal of Cell Biology, Vol. 175, No. 3, November 6, 2006 465–475
http://www.jcb.org/cgi/doi/10.1083/jcb.200605091

VBS that is capable of triggering vinculin activation, and that this VBS plays an essential role in *S. flexneri* pathogenesis.

Results

S. flexneri's invasin IpaA harbors two high-affinity VBSs

The VBSs of talin and α-actinin are amphipathic α helices (Izard and Vonrhein, 2004; Izard et al., 2004; Bois et al., 2005). IpaA binds to vinculin (Tran Van Nhieu et al., 1997; Bourdet-Sicard et al., 1999) through its C-terminal domain (IpaA-Cterm; IpaA residues 557–633; unpublished data). Therefore, we predicted that the ability of IpaA to bind to vinculin would be directed by an amphipathic α-helical VBS within this domain. Indeed, structure-based predictions revealed two potential amphipathic α helices in the IpaA-Cterm domain that might serve as VBSs. One, which we coined IpaA-VBS, was located at the C terminus of IpaA (residues 611–633; Fig. 1, A–C), whereas the second, IpaA-VBS2 (residues 565–587), is located only 24 residues N-terminal to IpaA-VBS (Fig. 1, A, B, and D).

To initially evaluate the role of the potential VBSs of IpaA in binding to vinculin, we generated strains of the *ipaA* deletion mutant of *Shigella flexneri* that were engineered to re-express wild-type IpaA protein (*ipaA/A*), or mutant IpaA proteins lacking IpaA-VBS (*ipaA/AΔVBS*; deletion of residues 589–633) or IpaA-VBS2 (*ipaA/AΔVBS2*; deletion of residues 565–586), or the entire C terminus of IpaA (*ipaA/AΔCterm*; lacking residues 559–633). All IpaA mutant proteins were secreted at levels similar to that of wild-type IpaA, as determined by Western blot analysis (Fig. 1 E). Wild-type and mutant IpaA proteins were tested for their ability to bind to vinculin in an overlay assay (Bourdet-Sicard et al., 1999). IpaA-ΔCterm failed to bind to vinculin, whereas binding to vinculin was detected for both IpaA-ΔVBS and -ΔVBS2 proteins (Fig. 1 E). Therefore, the C terminus of IpaA has two potential VBSs for vinculin, and either of them is sufficient to bind to vinculin.

To determine whether these potential VBSs of IpaA could also bind to vinculin in solution, we tested whether IpaA-VBS, -VBS2, or -Cterm could form stable complexes with recombinant Vh1 protein, as detected by native PAGE assays (Izard et al., 2004). Indeed, IpaA-VBS, -VBS2, or -Cterm readily formed stable, single complexes with the Vh1 domain of vinculin that were easily distinguishable from unbound Vh1 (Fig. 2 A). In contrast, a peptide comprised of the 23 residues linking the two IpaA-VBSs (IpaA-NB, for "nonbinder"; residues 588–610; Fig. 1 B) failed to bind to the Vh1 domain of vinculin (Fig. 2 A). Therefore, the two VBSs of IpaA can also bind to vinculin in solution.

To determine the affinity of IpaA-VBS versus -VBS2 for vinculin, and of the entire IpaA-Cterm domain, surface plasmon resonance (SPR) binding assays were performed. IpaA-VBS bound to the Vh1 domain of vinculin with very high-affinity (K_d of 0.11 nM; Fig. 2 B), 16–300-fold higher than that of the VBSs of talin and α-actinin (with K_ds ranging from 1.8 to 32.8 nM; Izard and Vonrhein, 2004; Bois et al., 2005, 2006). IpaA-VBS2 interacted with the Vh1 domain with a K_d of 6.61 nM (Fig. 2 C), which is comparable to the highest affinity VBS of talin (talin-VBS3; Izard and Vonrhein, 2004) and which approaches that

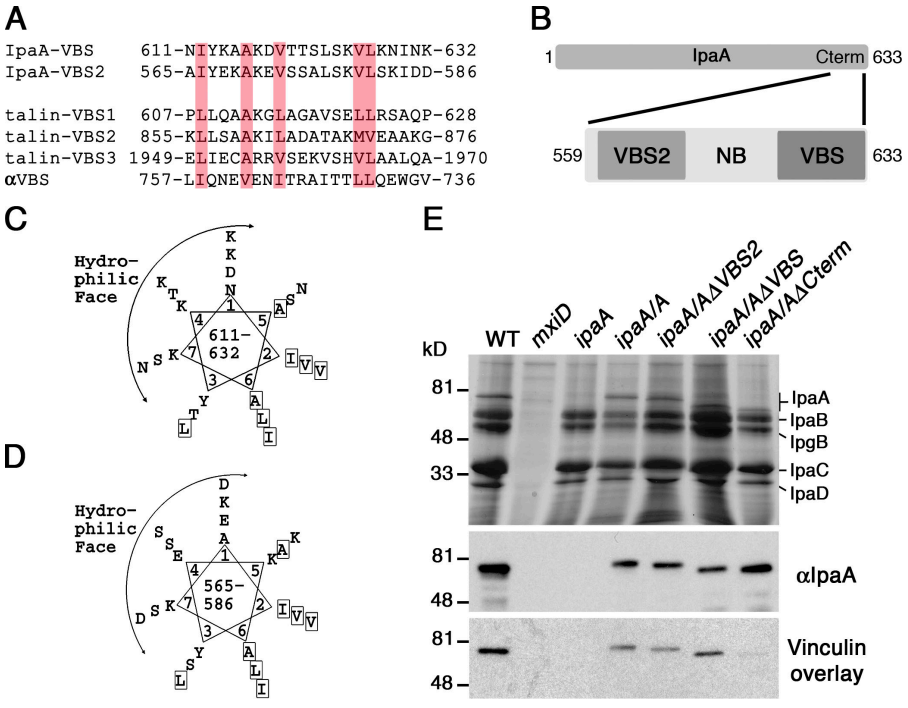

Figure 1. ***S. flexneri* IpaA harbors two putative VBSs (IpaA-VBSs).** (A) Structure-based sequence alignment of the complete IpaA amino acid sequence, using the Heidelberg PHD secondary-structure program, predicted that IpaA contains 66% α-helical character and identified two short regions, residues 563–589 and 612–630, which share strong similarity to the VBSs of talin and α-actinin. These putative IpaA VBSs, IpaA-VBS and -VBS2, were aligned with three of the VBSs of human talin (talin-VBS1, -VBS2, and -VBS3) and that of α-actinin (αVBS) using CLUSTAL protein software. As seen in the Vh1–αVBS structure (Bois et al., 2005), the orientation of the αVBS is inverted. Hydrophobic residues conserved in all five VBSs are shaded in pink. (B) Schematic of IpaA is shown and the C-terminal region of IpaA (residues 559–633), indicating the position and nomenclature of the peptides used in this study. (C) IpaA-VBS and (D) -VBS2 are predicted to be amphipathic α helices. The predicted IpaA-VBSs were arranged around a helical wheel, which revealed amphipathic helices having a hydrophilic basic face, and a hydrophobic face. Hydrophobic residues are boxed. (E) Either IpaA-VBS or -VBS2 is sufficient to bind to vinculin. Media from cultures of the indicated strains of *S. flexneri* were harvested and analyzed for the expression of *S. flexneri*'s invasin proteins, which were detected by staining SDS-PAGE gels with Coomassie blue (top). Samples were then blotted and levels of wild-type and mutant IpaA proteins were determined by Western blotting with IpaA-specific antibody (middle). Samples were also blotted with I^{125}-labeled vinculin using a vinculin overlay assay. Note that vinculin could bind to IpaA, IpaA-ΔVBS, and -ΔVBS2, but not to IpaA-ΔCterm, which lacks both of the VBSs of IpaA. The *mxiD* deletion (type III secretion system defective) does not secrete any of the invasin proteins (Perdomo et al., 1994).

estimated for the intramolecular head–tail interaction that clamps vinculin in its inactive state (Cohen et al., 2005). Nonetheless, the affinity of IpaA-VBS2 for Vh1 was still 60-fold lower than that of IpaA-VBS for the N-terminal domain of vinculin. Strikingly, SPR analyses with IpaA-Cterm showed an even higher affinity for vinculin as, quite remarkably, the K_d of the Vh1–IpaA-Cterm interaction was 6.2 femtomolar, and the K_d of the IpaA-Cterm interaction with full-length vinculin was 35.2 picomolar (Fig. 2, D and E). Furthermore, off-rate analysis demonstrated that, once bound to the Vh1 domain of vinculin, IpaA-Cterm essentially did not dissociate (Fig. 2 F), and that it also had a very slow off-rate for full-length vinculin (Fig. 2 G). Indeed, the affinity of the IpaA-Cterm domain for vinculin is approximately two orders of magnitude greater than that reported for any other binding partner of vinculin, including the low nanomolar affinity of the intramolecular interaction of vinculin's head and tail domains, which clamp vinculin in its inactive state (Cohen et al., 2005).

IpaA-VBSs determine vinculin recruitment at bacterial-induced actin foci

To test the effects of *S. flexneri*'s IpaA-VBSs on IpaA function, we analyzed the invasion and cell–cell dissemination of wild-type *S. flexneri* (strain M90T; Perdomo et al., 1994) and *ipaA* mutant *S. flexneri* strains complemented with full-length IpaA (*IpaA/A*), or IpaA derivatives lacking the IpaA-Cterm domain (*ΔCterm*), the IpaA-VBS (*ΔVBS*), or the IpaA-VBS2 (*ΔVBS2*). We first tested if IpaA translocation into infected HeLa cells was comparable between the *ipaA/A* strain and mutant IpaA strains by immunoprecipitating translocated IpaA derivatives from lysates of HeLa cells infected with the various *S. flexneri* strains. As negative controls, we used the *ipaA* deletion mutant

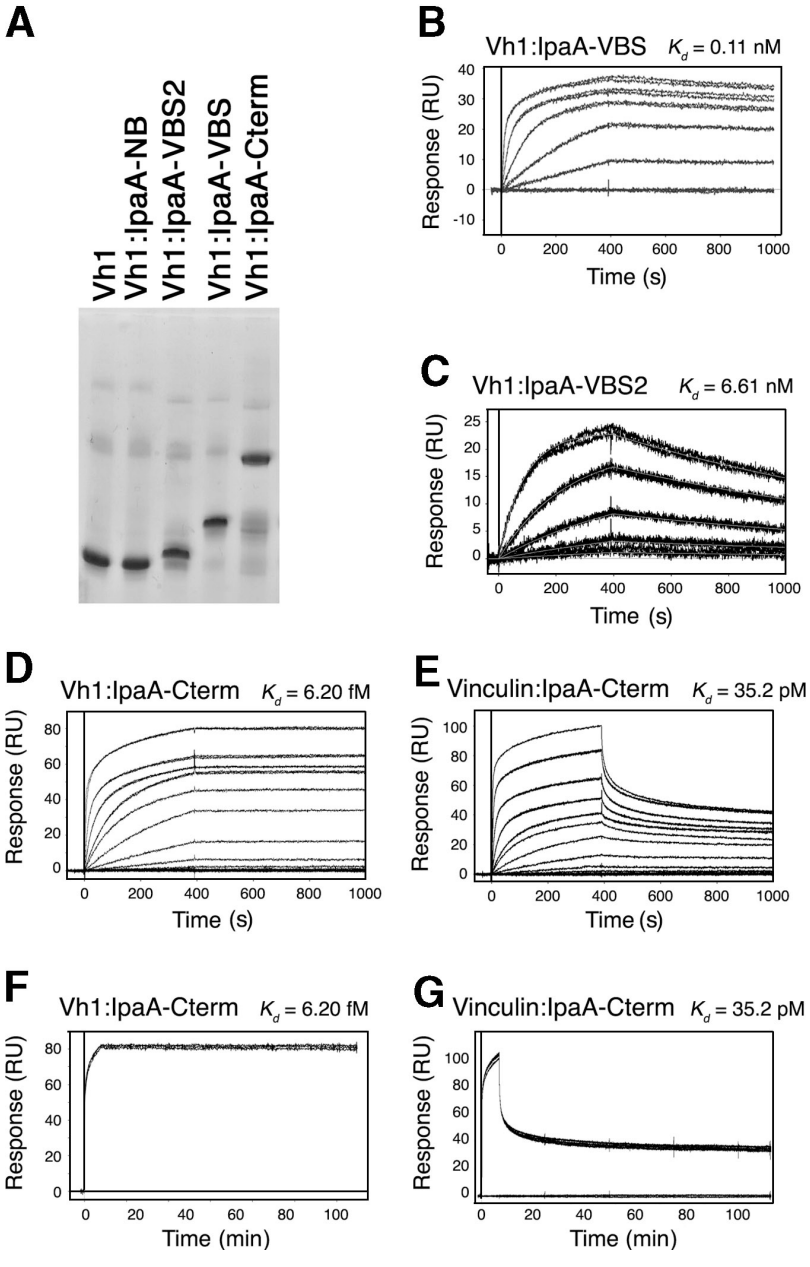

Figure 2. ***S. flexneri*'s IpaA protein harbors high-affinity VBSs.** (A) Native gel analyses of free Vh1, or Vh1 incubated with IpaA-NB, -VBS2, -VBS, or -Cterm. (B–E) SPR of the affinity of IpaA-VBS (B), -VBS2 (C), or -Cterm (D and E) for Vh1 (B, C, and D) or for full-length human vinculin (E). Representative sensorgrams are shown. The calculated K_d is shown above each panel. (F and G) Off-rate analyses of the (F) Vh1–IpaA-Cterm and (G) vinculin–IpaA-Cterm interactions over a time course of >100 min are shown. Representative sensorgrams from three independent experiments are shown.

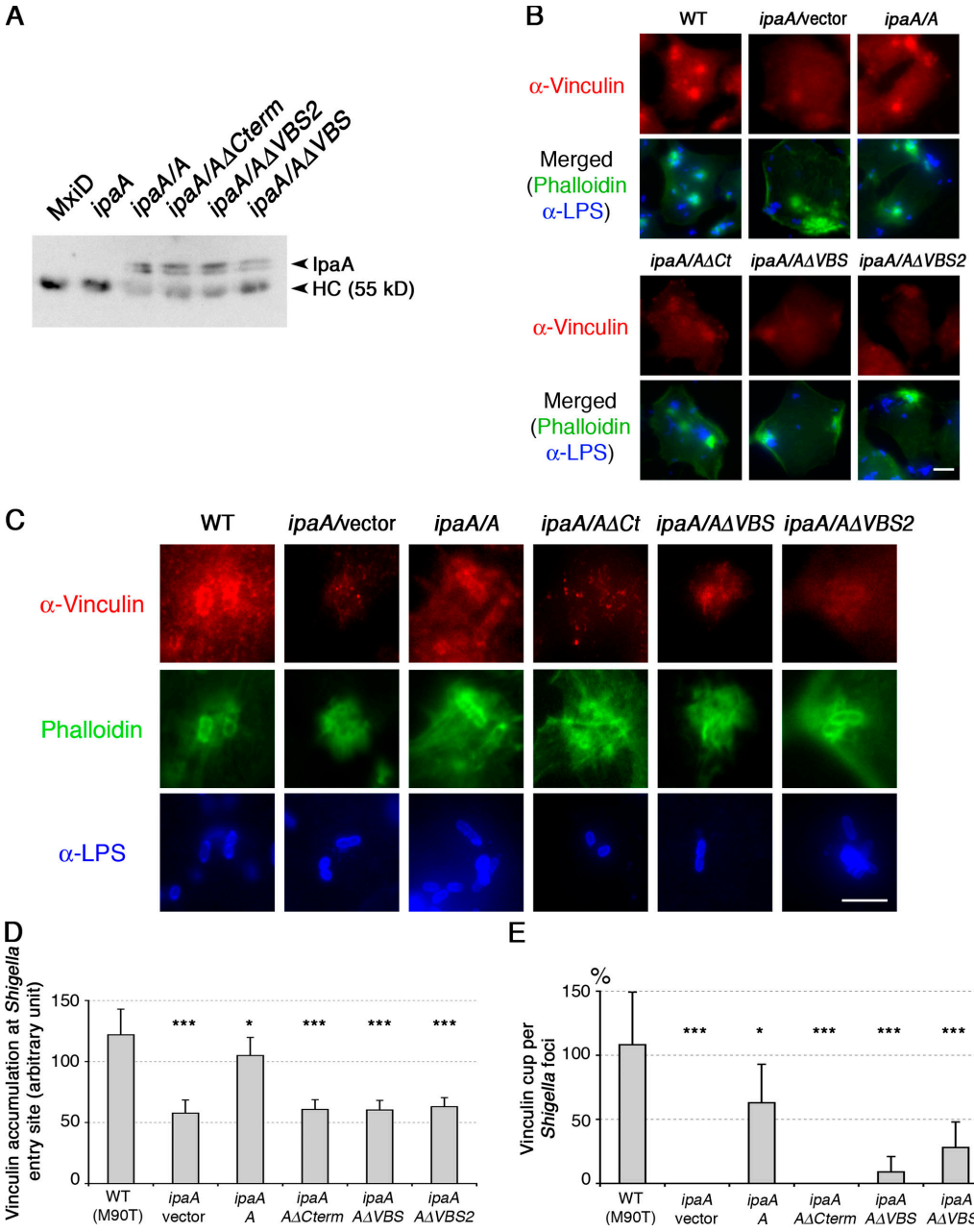

Figure 3. **The VBSs of IpaA recruit vinculin to *S. flexneri* at bacterial entry sites.** (A) The VBSs of *S. flexneri* are dispensable for translocation of IpaA into infected cells. Lysates of HeLa cells infected with equal multiplicities of infection of the indicated strains of *S. flexneri* were evaluated for their levels of intracellular IpaA protein using anti-IpaA antibody complexed to G–Sepharose, SDS-Page, and Western blotting with anti-IpaA antibody. IpaA protein appeared as a doublet, suggesting that some *IpaA* degradation occurred. *IpaA* and the antibody heavy chain (HC; loading control) are indicated. (B) Immunofluorescence analyses of vinculin (red), LPS (blue), and actin (phalloidin; green) in HeLa cells infected with the indicated strains of *S. flexneri* is shown. Vinculin is effectively recruited to wild-type and *ipaA/A S. flexneri* at entry foci, whereas this does not occur in HeLa cells infected with the *S. flexneri ipaA* deletion strain, nor in HeLa cells infected with the *S. flexneri ipaA/AΔCterm* (Ct), *ipaA/AΔVBS*, and *ipaA/AΔVBS2* strains. Actin foci containing vinculin are evident in HeLa cells infected with the *ipaA, ipaA/AΔCt, ipaA/AΔVBS*, and *ipaA/AΔVBS2* strains of *S. flexneri*. Note that infection of HeLa cells with wild-type *S. flexneri* or strains expressing the IpaA mutants did not overtly disrupt focal adhesions, which were still evident in cells stained with anti-vinculin antibody, and which are consistent with the lack of appreciable effects of the VBSs of IpaA in displacing vinculin–talin interactions (Fig. 5, C, D, and F). (C) Vinculin (red) recruitment to internalized bacteria (anti-LPS; blue) is observed in HeLa cells infected with wild-type and *ipaA/A* strains of *S. flexneri*, where vinculin (and actin) appears to coat the surface of their membranes. Reduced vinculin staining of the bacterium was observed with *ipaA/AΔVBS* and *ipaA/AΔVBS2 S. flexneri*, and was not detected in cells expressing the *ipaA* deletion strain or the *ipaA/AΔCt* strain of *S. flexneri*. Images correspond to "maximum" reconstructions from z planes delimitating *S. flexneri* entry sites using the Metamorph software (see Materials and methods). (D) Quantification of total vinculin recruitment at entry sites of *S. flexneri* was determined using the MetaMorph software. (E) The percentages of bacteria decorated with vinculin at entry foci were quantified. A minimum of 56 foci were scored for each strain (mean of 100). Error bars indicating the mean ± the SEM are provided together with the *t* test P value (*, $P < 0.05$; **, $P < 0.005$; and *** P, < 0.0005).

S. flexneri strain, as well as the *mxiD* (deficient type III secretion apparatus) mutant strain, which, as expected, did not show any *ipaA* translocated into HeLa cells. Although, as observed for other translocated type III effectors (Kubori and Galán, 2003), some degradation of IpaA proteins was observed, the overall levels of the IpaA-ΔVBS, -ΔVBS2, and -ΔCterm proteins in infected HeLa cells were similar to those of wild-type IpaA protein in HeLa cells infected with the *ipaA/A* strain (Fig. 3 A).

To determine the roles of the VBSs of IpaA in the recruitment of vinculin during bacterial entry, we assessed vinculin localization at sites of *S. flexneri* entry by immunofluorescence assays. As expected, vinculin was efficiently recruited to bacterial-induced actin foci in HeLa cells infected with wild-type *S. flexneri* or with the *ipaA/A* strains, but was not recruited to actin foci in cells infected with the *ipaA* mutant (Fig. 3 B). Interestingly, vinculin was also not recruited to actin foci in cells infected with the *ipaA/ΔCterm*, *ipaA/ΔVBS*, or *ipaA/ΔVBS2* strains (Fig. 3, B and D), indicating that both VBSs are required for efficient recruitment at bacterial entry sites. Although quantification of the average intensity of vinculin staining at sites of actin foci confirmed the deficiency of vinculin recruitment in cells infected with the *ipaA/ΔCterm*, *ipaA/ΔVBS*, or *ipaA/ΔVBS2* strains (Fig. 3 C), there were also differences in the sublocalization of vinculin observed at entry foci induced by the *ipaA/ΔVBS2*, *ipaA/ΔCterm*, and *ipaA/ΔVBS* strains (Fig. 3 C). This difference was most clearly apparent in the formation of the "actin cup" that normally surrounds the internalized pathogen (Tran Van Nhieu et al., 1997), and which is also characterized by intense vinculin staining around the internalized bacterium (Fig. 3 C, WT and *ipaA/A*). Notably, actin–vinculin cups around the internalized bacterium were not observed in cells infected with the *ipaA/ΔCterm* strain, and these were reduced, by 10- or 4-fold, in cells infected with the *ipaA/ΔVBS* and *ipaA/ΔVBS2* strains, respectively (Fig. 3 C). Therefore, IpaA-VBS and -VBS2 of *S. flexneri* are both essential for efficient recruitment of vinculin to bacterial actin foci at *S. flexneri* entry sites (Fig. 3 C), whereas the IpaA-VBS plays a more important role in recruiting vinculin to the actin cups that surround the internalized pathogen (Fig. 3, D and E).

The IpaA-VBS is essential for efficient host cell entry and spread of *S. flexneri*

We next tested whether *S. flexneri*'s IpaA mutants were compromised in their ability to invade the host cell by performing gentamicin protection assays (Isberg and Falkow, 1985). Notably, the *ΔCterm* and *ΔVBS* deletion mutants were markedly impaired in their ability to invade HeLa cells compared with wild-type *S. flexneri* or the *ipaA* deletion strain engineered to reexpress IpaA (*ipaA*/*A*; Fig. 4 A). In contrast, the *ipaA*/*AΔVBS2* strain was as effective as wild-type *S. flexneri* and the *ipaA*/*A* strain in cell entry (Fig. 4 A). The reduction in bacterial invasion linked to these mutations was, however, not as drastic as that observed for the *ipaA* mutant strain, indicating that in addition to the IpaA C terminus, other domains of IpaA also contribute to bacterial invasion.

During replication in epithelial cells, *S. flexneri* disseminates from cell to cell using actin-based motility (Gouin et al., 2005). To further address the role of the VBSs of IpaA in invasion and also in cell–cell spread, we performed a modified plaque assay on polarized monolayers of Caco-2 colon epithelial cells. In this assay, exposure of the monolayers to low bacterial multiplicities of infection leads to discrete entry events, which are visualized as bacterial plaques after a 6-h incubation in the presence of gentamicin. This prevents de novo invasion yet allows for bacterial dissemination to neighboring cells. Thus, the frequency of plaque formation reflects bacterial

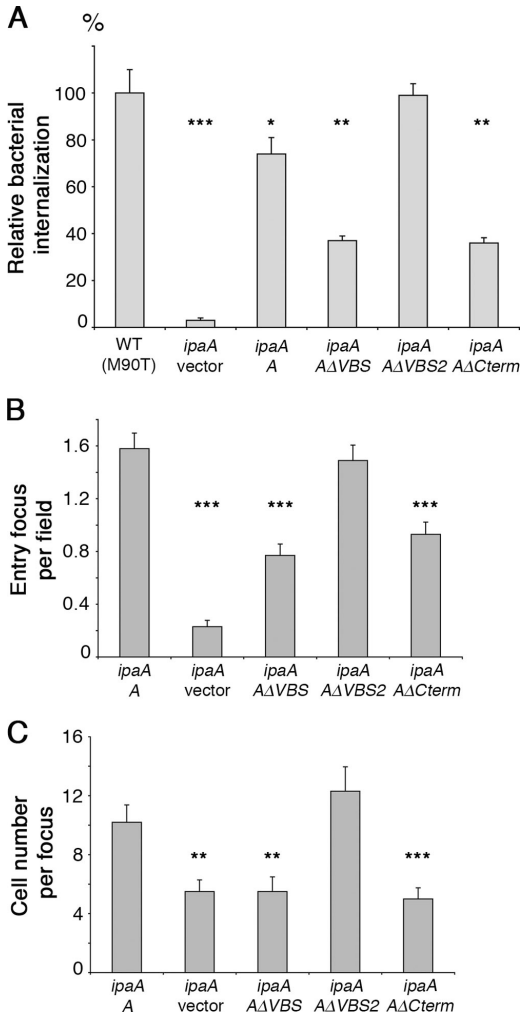

Figure 4. ***S. flexneri*'s IpaA-VBSs contribute to host cell entry and to dissemination of the pathogen.** (A) Deletion of IpaA-VBS compromises the invasion of HeLa cells by *S. flexneri*. HeLa cells were challenged with the indicated strains and bacterial internalization was determined by the gentamicin protection assay (Perdomo et al., 1994). The relative percentage of bacterial internalization corresponds to values normalized to that obtained for the wild-type strain. Each value is the mean of six independent determinations. (B) Polarized colonic epithelial Caco-2 cells were challenged with the indicated mutants, and bacterial internalization was assessed by scoring entry events by fluorescent microscopy. (C) Deletion of IpaA-VBS affects *S. flexneri* dissemination. Polarized Caco-2 cells were challenged with the indicated mutants for 90 min, and bacterial dissemination after a 6-h incubation was determined by scoring the numbers of infected cells per focus. Error bars indicating the mean ± the SEM are provided together with the *t* test P value (*, $P < 0.05$; **, $P < 0.005$; and *** P, < 0.0005).

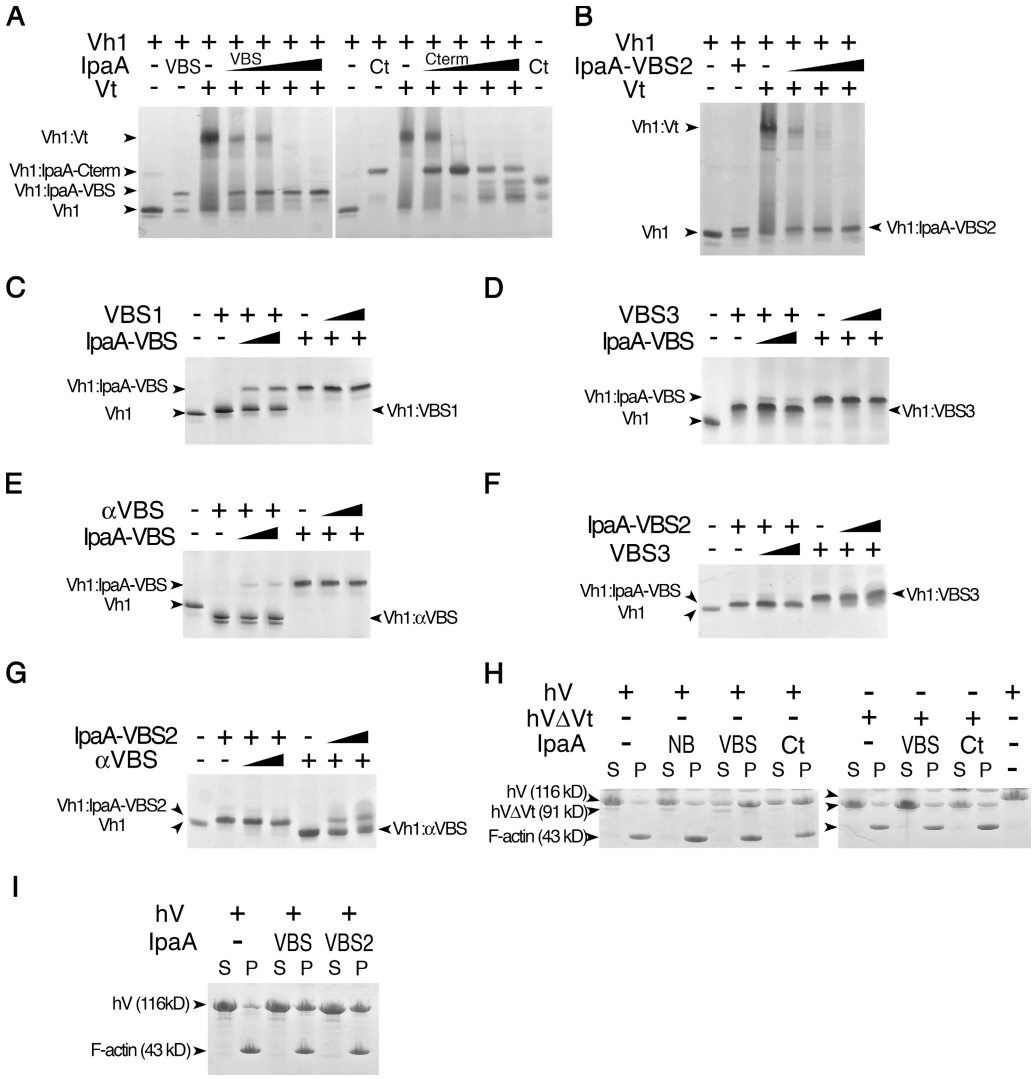

Figure 5. ***S. flexneri*'s IpaA-VBSs activate vinculin.** (A) *S. flexneri's* IpaA-VBSs and its C-terminal domain (Ct) sever the Vh1–Vt interaction that clamps vinculin in its inactive state (Borgon et al., 2004; Izard et al., 2004). Lane 1 in both the left and right native gels show Vh1 alone, and lane 2 shows the Vh1–IpaA-VBS complex (left) or the Vh1–IpaA-Cterm complex (right). The + denotes the addition of the indicated IpaA domain to preformed Vh1–Vt complexes. Competing IpaA-VBS (left) was titrated (lanes 4–7, arrowheads) into preformed Vh1–Vt complexes at molar ratios of IpaA-VBS at ∼2-, 3.5-, 10-, and 20-fold molar ratios (Vh1–IpaA-VBS). Competing IpaA-Cterm peptide (right) was titrated (arrows) into preformed Vh1–Vt complexes at 0.9-, 1.7-, 3.4-, and 6.8-fold molar ratios (Vh1–IpaA-Cterm). As is evident, titration of even very low molar ratios of IpaA-VBS or IpaA-Cterm was sufficient to totally disrupt the Vh1–Vt complex to form novel Vh1–IpaA-VBS (left) or Vh1–IpaA-Cterm (right) complexes. Because of its basic pI, free Vt is not visible in native gels (Izard et al., 2004). (B) IpaA-VBS2 is also sufficient to disrupt the Vh1–Vt interaction. Native gel analyses of free Vh1 (lane 1), Vh1 in complex with IpaA-VBS2 (lane 2), Vh1–Vt complex (lane 3), or preexisting Vh1–Vt complexes titrated with increasing concentrations of IpaA-VBS2 (at ∼2-, 3.5-, 10-, and 20-fold molar ratios; Vh1–IpaA-VBS2). The identity of the complexes is shown. (C–G) The selective nature of the IpaA–vinculin interaction. Reciprocal VBS displacement native gel assays of Vh1 in complex with talin-VBS1 (C), talin-VBS3 (D and F), or the VBS of α-actinin (αVBS; E and G) versus when in complex with IpaA-VBS (C–E) or IpaA-VBS2 (F and G). Competing IpaA-VBS, IpaA-VBS2, talin-VBS3, talin-VBS1, or αVBS peptides were titrated (arrows) into preformed complexes at 2.2- or 10-fold molar excess (Vh1–VBS). Native gels of the indicated complexes are shown. (H and I) IpaA-VBS (H) and -VBS2 (I) promote vinculin binding to F-actin. IpaA-NB, -VBS (VBS), -VBS2 (VBS2), or -Cterm (Ct) were incubated with full-length human vinculin (hV) or human vinculin lacking the tail domain Vt (hVΔVt), which mediates binding to F-actin (Johnson and Craig, 1995). Samples were incubated with F-actin, as previously described (Bois et al., 2006), and centrifuged into pellet (containing polymerized F-actin) and supernatant fractions, and then equal volumes were analyzed by SDS-PAGE. F-actin and vinculin were visualized by staining the gels with Coomassie blue. The last lane on the right of H shows the size difference between full-length vinculin (residues 1–1,066) and the head domain of vinculin (residues 1–840).

invasion, whereas bacterial dissemination is assessed by quantifying the number of infected cells per plaque (Tran Van Nhieu et al., 2003). When invasion was analyzed by counting plaques induced by the various strains on polarized monolayers, results similar to those in HeLa cells were obtained, with the *ipaA/AΔVBS2* strain forming essentially as many plaques as the *ipaA/A* strain, whereas the *ipaA/AΔVBS* and *ipaA/ΔCterm* strains showed a similar twofold reduction in plaque frequency (Fig. 4 B). Remarkably, analysis of bacterial dissemination provided results that paralleled invasion. Plaques formed by the *ipaA* mutant contained two times less infected cells than the *ipaA/A* strain (Fig. 4 C). Importantly, the *ipaA-ΔCterm* or *ipaA-ΔVBS* mutant strains were as defective in their dissemination as the *ipaA* strain lacking IpaA. In contrast, the spread of

the *ipaA/AΔVBS2* strain was similar to that of the *ipaA/A* strain that expresses wild-type IpaA (Fig. 4 C). Therefore, IpaA-VBS, but not IpaA-VBS2, plays an important role for entry into the host cell, and for cell–cell spread of *S. flexneri*.

S. flexneri's IpaA-VBSs activate vinculin

The high affinity of IpaA-VBS or -VBS2 for vinculin, and their sequence similarity with the VBSs of talin and α-actinin (Fig. 1 A), suggested that, like the VBSs of talin and α-actinin (Izard et al., 2004; Izard and Vonrhein, 2004; Bois et al., 2005, 2006), *S. flexneri*'s IpaA-VBSs might also be sufficient to sever vinculin's head–tail interactions, which normally clamp the molecule in its inactive conformation (Bakolitsa et al., 2004; Borgon et al., 2004; Izard et al., 2004). Indeed, native gel analyses demonstrated that relatively low molar ratios of either IpaA-VBS, -VBS2, or -Cterm were sufficient to completely displace Vt from preexisting Vh1–Vt complexes (Fig. 5, A and B). Therefore, the VBSs of IpaA are sufficient to disrupt the intramolecular head–tail interactions of vinculin, which is the initiating event of vinculin activation (Johnson and Craig, 1995; Gilmore and Burridge, 1996).

The VBSs of talin and α–actinin bind to vinculin in a mutually exclusive manner and can efficiently displace one another from preexisting complexes with Vh1 (Izard et al., 2004). The very high affinity of *S. flexneri*'s IpaA-VBSs for vinculin (Fig. 2), however, suggested that the interaction of the VBSs of IpaA with vinculin in solution might be resistant to displacement by the VBSs of talin or α-actinin. Indeed, the VBSs of talin (VBS1 and VBS3) and α-actinin (αVBS) were not capable of displacing IpaA-VBS from preexisting Vh1–IpaA-VBS complexes (Fig. 5, C–E). Similarly, despite a 60-fold lower affinity of IpaA-VBS2 for vinculin (Fig. 2 C), talin-VBS3 and αVBS were not capable of displacing IpaA-VBS2 from preexisting Vh1–IpaA-VBS2 complexes (Fig. 5, F and G). Therefore, once bound, IpaA would be predicted to compromise contacts of vinculin with its endogenous partners. Surprisingly, IpaA-VBS and -VBS2 were relatively ineffective at displacing talin-VBS1, talin-VBS3, or αVBS from preexisting Vh1–talin-VBS1,–talin-VBS3, or –αVBS complexes (Fig. 5, C–G). These results suggest that *S. flexneri*'s IpaA protein would preferentially interact with pools of free vinculin, rather than with vinculin bound by talin or α-actinin at sites of focal adhesions or adherens junctions.

A hallmark of vinculin activation is its ability to bind to F-actin (Johnson and Craig, 1995), and IpaA activates this latent binding activity (Bourdet-Sicard et al., 1999). To address the role of IpaA-VBS and IpaA-VBS2 in this process, we used F-actin cosedimentation assays (Bois et al., 2006). Although native vinculin or vinculin incubated with the IpaA-NB peptide failed to bind to F-actin, IpaA-VBS–, IpaA-VBS2–, or IpaA-Cterm–bound vinculin efficiently cosedimented with F-actin (Fig. 5, H and I). Finally, neither IpaA-VBS or IpaA-Cterm contained a cryptic F-actin–binding domain, as IpaA-VBS or IpaA-Cterm bound to a vinculin mutant that lacks its actin-binding tail domain (hVΔVt; human vinculin residues 1–840; Bois et al., 2006) failed to cosediment F-actin (Fig. 5 H). Therefore, the VBSs of IpaA, and its C-terminal domain, are sufficient to promote binding of vinculin to F-actin.

S. flexneri's IpaA-VBSs mimic talin to bind to and activate vinculin

The amphipathic α-helical nature of the VBSs of IpaA, their high-affinity binding to vinculin, and their similarity to the VBSs of talin and α-actinin in displacing the head–tail interaction of vinculin, suggested they might bind to vinculin in a manner akin to talin or α-actinin. The VBSs of talin and α-actinin insert between Vh1 helices α1 and α2, and make extensive hydrophobic contacts with Vh1 helices α1, α2, and α4 that provoke drastic changes in its structure, displacing Vt from a distance (Izard et al., 2004; Izard and Vonrhein, 2004; Bois et al., 2005; Fillingham et al., 2005). To determine the precise nature of the IpaA–vinculin interaction, we solved the crystal structure the Vh1 domain in complex with IpaA residues 602–633 (containing the IpaA-VBS; Fig. 6 A, and Tables S1 and S2, available at http://www.jcb.org/cgi/content/full/jcb.200605091/DC1), as well as with IpaA residues 565–587 (IpaA-VBS2; Fig. 6 B and Tables S3 and S4). These structures established that IpaA-VBS and -VBS2 are indeed amphipathic α helices (Fig. 6), confirming their sequence alignments (Fig. 1 A) and predictions of their secondary structure (Fig. 1, C and D). Both IpaA-VBS and -VBS2 bind to the Vh1 domain of vinculin in an intimate fashion, largely through van der Waals interactions, where the hydrophobic faces of these VBSs interact with the hydrophobic core of the N-terminal four-helical bundle subdomain of Vh1 (Fig. 6), events that would displace Vt's interactions with the Vh1 domain from a distance.

The structural alterations provoked by the binding of the IpaA-VBSs to vinculin were reminiscent of those induced by the binding of the VBSs of talin and α-actinin, which produce dramatic changes in the structure of the Vh1 domain, yet bind to Vh1 in an inverted orientation and provoke unique conformational changes in full-length vinculin (Izard and Vonrhein, 2004; Izard et al., 2004; Bois et al., 2005). Superposition revealed that IpaA-VBSs behaved as striking and selective mimic of talin's VBSs in altering the structure of vinculin (Fig. 6). Therefore, *S. flexneri* applies molecular mimicry of talin to bind to and activate vinculin.

The unusual behavior of *S. flexneri*'s IpaA-VBSs in displacement assays with talin– or α-actinin–VBS–bound vinculin, and their higher affinity for vinculin, suggested there might be some unique features of their hydrophobic interactions with the Vh1 domain of vinculin. Indeed, inspection of their structures established that Phe-126 of vinculin interacts with Tyr-613 or -567 of IpaA-VBS or -VBS2, respectively (Fig. S2 A, available at http://www.jcb.org/cgi/content/full/jcb.200605091/DC1), whereas the interaction of vinculin Phe-126 with the VBSs of talin are through interactions with small, aliphatic sidechains (Fig. 1 A). To test our hypothesis that the presence of Tyr-613 (IpaA-VBS) and -567 (IpaA-VBS2) strengthened their binding to Vh1, we synthesized mutant IpaA-VBS and -VBS2 peptides where these tyrosine residues were replaced by isoleucine residues as seen in talin-VBS3 (Fig. 1 A; Ile-1950; Fig. S2 A). SPR analysis showed a decrease in the affinity of the mutant peptides for Vh1, where the K_d of IpaA-VBS for Vh1 was reduced from 0.11 (WT) to 0.27 nM (Y613I), and where the K_d of IpaA-VBS2 was reduced from 6.61 (WT) to 15 nM (Y567I). Furthermore,

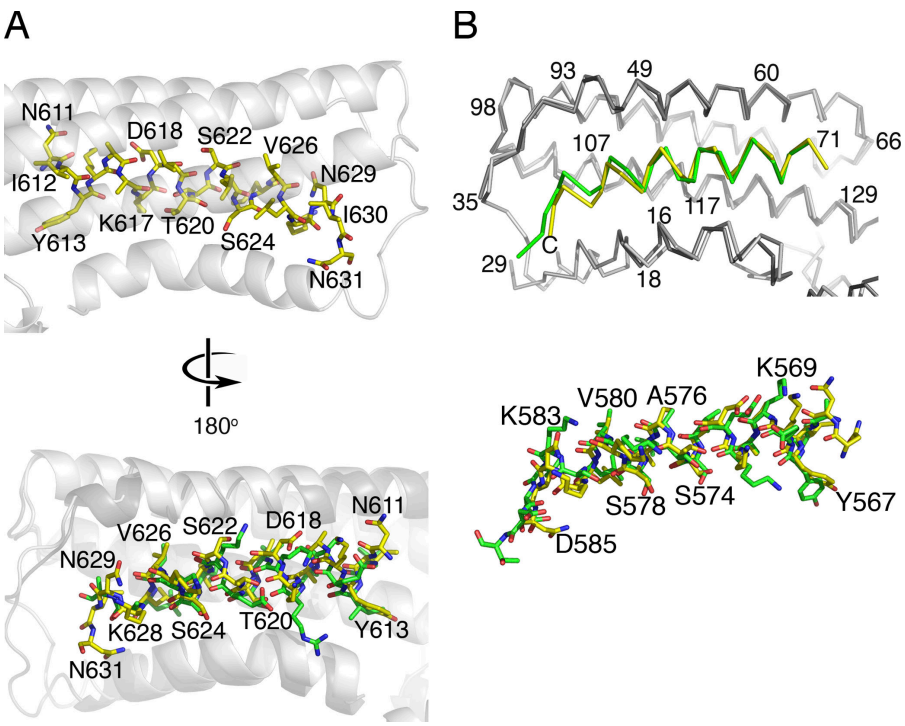

Figure 6. **The mechanism of vinculin activation by *S. flexneri*'s IpaA protein.** (A, top) The crystal structure of the Vh1–IpaA-VBS complex showing the hydrophobic face of IpaA-VBS (yellow bonds; some residues are labeled) that interacts with vinculin (transparent white helices). Vinculin is shown as a ribbon diagram in white, and the individual bonds are drawn in yellow for IpaA-VBS (oxygen atoms, red; carbon, yellow; nitrogen, blue). (bottom) Superposition of talin-VBS3 (green bonds) onto IpaA-VBS (yellow bonds) bound to vinculin (white and gray, respectively). This orientation is rotated by 180° in respect to the top image showing the hydrophilic solvent–exposed face of these VBSs. Some IpaA-VBS residues are labeled. (B) (top) The Cα trace of the Vh1 domain of vinculin bound to IpaA-VBS (yellow) superimposed onto IpaA-VBS2 (green) bound to Vh1 in gray (Vh1–IpaA-VBS2) or white (Vh1–IpaA-VBS). Some vinculin residues are labeled. (bottom) Ball-and-stick representation of the structure of IpaA-VBS (yellow) superimposed onto that of IpaA-VBS2 (green); some residues of IpaA-VBS2 are labeled. Both images are shown in the same orientation.

comparison of the Vh1–IpaA-VBS and Vh1–IpaA-VBS2 crystal structures revealed that the sidechain of Lys-569 was near the IpaA-VBS2–vinculin interface, where it could potentially sterically interfere with binding. Indeed, mutating lysine-569 to an alanine (as seen in IpaA-VBS Ala-615; Fig. 1 A, Fig. 6 B, and Fig. S2 B) converted IpaA-VBS2 into a much stronger VBS as assessed by SPR assays, where the K_d of IpaA-VBS2 K569A was 0.53 nM, which is an order of magnitude higher than wild-type IpaA-VBS2 (6.61 nM). Therefore, at least two residues of the IpaA-VBS, Tyr-613 and Ala-615, contribute to its unique, very high-affinity interactions with the hydrophobic interface with vinculin.

Discussion

The Gram-negative pathogens *S. flexneri* and *Salmonella enterica* gain passage into the host cell through the agency of a type III secretion apparatus that jettisons invasin proteins into the host cell, which then act in concert to reorganize the actin cytoskeleton to direct entry and intercellular spread of these pathogens. *S. flexneri* invasion requires IpaA and its cellular target vinculin (Tran Van Nhieu et al., 1997), which together reorganize the actin cytoskeleton to allow completion of the *S. flexneri* entry process (Bourdet-Sicard et al., 1999). This strategy differs from that used by *Salmonella*, where its SipA actin-binding protein stabilizes actin filaments to promote formation of filopodial extensions and membrane ruffles that together engulf the pathogen (Zhou et al., 1999; Lilic et al., 2003; McGhie et al., 2004). Nonetheless, it is now clear that a shared strategy of all Gram-negative pathogens is to subvert the actin cytoskeleton to gain purchase within the host (Stebbins and Galán, 2001; Galkin et al., 2002).

The data presented clearly demonstrate that, using evolutionary convergence, *S. flexneri* has engineered two VBSs that modulate the structure and function of vinculin by using a remarkable level of mimicry of the VBSs of talin. This is most strikingly shown by the crystal structures of the VBSs of IpaA in complex with vinculin, which also bind to vinculin in the same orientation as the VBSs of talin (Fig. 6). However, our structural and biochemical studies have indicated that there are unique features of the IpaA–vinculin interaction that might explain the high affinities of the VBSs of IpaA (Fig. 2) and their rather unusual behavior in displacement assays (Fig. 5), and it is possible that these differences could be exploited for deriving new therapeutics to treat and/or protect humans from this devastating pathogen.

Although the proteins of other pathogens have been shown to be mimic other components and regulators of the actin cytoskeleton (Stebbins and Galán, 2001), thus far *S. flexneri* is unique in that one of its invasins functions as a talin mimic to invade the host cell and to recruit vinculin to sites of bacterial entry. Furthermore, the requirement for the IpaA-VBS–vinculin interaction in cell–cell dissemination suggests that IpaA alters vinculin functions in unique ways that allow for intercellular motility of *S. flexneri*, possibly through influencing vinculin–Arp2/3 complexes that are required for spread of the pathogen (Loisel et al., 1999; Gouin et al., 2005).

The most C-terminal VBS of IpaA, IpaA-VBS, functions by all measurable criteria as a bona fide trigger that activates vinculin. First, IpaA-VBS has a remarkably high affinity for vinculin (Fig. 2), at least 10-fold higher than any other VBS (e.g., the αVBS of the α-actinin–vinculin interaction has a K_d of ∼1.8 nM; Bois et al., 2005), and the femtomolar–picomolar affinities of the C terminus of IpaA for vinculin indicate that once

vinculin is bound by IpaA, it cannot be displaced by the binding of vinculin's other partners, a notion supported by VBS displacement assays (Fig. 5). Furthermore, IpaA-VBS can efficiently sever vinculin's head–tail interaction and trigger the latent F-actin–binding activity of vinculin (Fig. 5), both hallmarks of vinculin activation (Johnson and Craig, 1995; Gilmore and Burridge, 1996). Finally, and most importantly, the IpaA-VBS plays critical roles in directing host cell entry and dissemination of *S. flexneri* (Fig. 4).

At face value, the second VBS of IpaA, IpaA-VBS2, would also appear to have all the hallmarks of a trigger that should activate vinculin in cells, especially given its ability to sever the vinculin head–tail interaction and to promote F-actin binding (Fig. 2). However, in tests of its biological activity, IpaA-VBS2 appeared less critical than IpaA-VBS for cell entry and dissemination of *S. flexneri*. However, possible clues to the potential function and relevance of *S. flexneri* having these two VBSs have come from further revelations regarding the overall scope of the interactions between *S. flexneri* and vinculin (Fig. 3). Although IpaA and vinculin were known to interact locally at sites of pathogen–host contact, and to provoke changes in the actin cytoskeleton to form the pseudoadhesion complex or the actin cup that forms around the internalized bacterium (Trans Van Nhieu and Ben-Ze'ev, 1997; Trans Van Nhieu et al., 2000), this interaction clearly requires the functions of both of the VBSs of IpaA. Strikingly, however, IpaA-VBS appears to play a more crucial role than IpaA-VBS2 in recruiting vinculin, a finding that is consistent with the estimated 60-fold difference in affinity. Thus, the two VBSs of *S. flexneri*'s IpaA protein appear to facilitate both the recruitment of vinculin at sites of bacterial entry, and in forming the actin-vinculin cup that surrounds the membranes of the internalized pathogen. The precise role that this highly effective recruitment of vinculin by the VBSs of IpaA is unclear because recruitment mediated by IpaA-VBS alone appears sufficient for bacterial invasion and cell–cell spread in epithelial cells in vitro. It is possible, however, that more efficient vinculin recruitment mediated by both of the VBSs of IpaA becomes critical for invasion of enterocytes during in vivo infection.

Materials and methods

Protein preparation and purification
Human full-length vinculin (residues 1–1,066), vinculin lacking its tail domain (residues 1–840), and the Vh1 (residues 1–258) and Vt (residues 879–1,066) domains of vinculin were purified as previously described (Borgon et al., 2004; Izard et al., 2004; Bois et al., 2006). The IpaA-Cterm (residues 559–633) protein was expressed in *E. coli* as a GST fusion protein using a pGEX expression construct (Novagen). Cells were lysed in PBS and PMSF, and the protein was purified using a glutathione–Sepharose affinity column, GST cleavage, and anion exchange chromatography (Q–Sepharose). Human αVBS (residues 731–760), talin-VBS1 (residues 607–636), or talin-VBS3 (residues 1,949–1,970), the six wild-type IpaA-VBSs of varying lengths, and a nonbinding IpaA peptide, as well as the three mutant IpaA-VBSs (IpaA-VBS-Y613I [NIIKAAKDVTTSLSKVLKNINKD], IpaA-VBS2-Y567I [AIIEKAKEVSSALSKVLLSKIDDT], and IpaA-VBS2-K569A [AIYEAAKEVSSALSKVLSKIDDT]) were synthesized and HPLC purified in our in-house facility.

SPR studies
Binding studies were performed by SPR using a biosensor (Biacore 2000; Biacore) equipped with a carboxymethyldextran-coated gold surface (CM-5) sensor, as previously described (Izard and Vonrhein, 2004).

Vinculin-IpaA gel retardation assays
65 nM Vh1 protein was incubated with IpaA-VBS2, -NB (nonbinder), -VBS, or -Cterm (Fig. 2 A) in PBS at room temperature using an ∼1:2 molar ratio of Vh1/IpaA. Complexes were run on 20% homogeneous native polyacrylamide PhastGels (GE Healthcare). Protein detection was performed using Coomassie blue staining. Only a single Vh1–IpaA-Cterm complex was detected, indicating that IpaA-Cterm protein, at this molar ratio, interacted with Vh1 with a 1:1 stoichiometry.

Vinculin and Vh1–VBS displacement assays
All binding assays were performed in PBS buffer. 130 nM Vh1 protein was added to Vt at room temperature using a ∼1:2 molar ratio of Vh1/Vt (i.e., Vt at 260 nM), to ensure that all Vh1 was in complex with Vt. Analysis on native polyacrylamide gels confirmed formation of the Vh1–Vt complex. IpaA-VBS, -VBS2, or -Cterm were added to the Vh1–Vt complex. IpaA-VBS was titrated at ∼2-, 3.5-, 10-, and 20-fold molar ratios, and IpaA-Cterm was titrated at 0.9-, 1.7-, 3.4-, and 6.8-fold molar ratios. Complexes formed were resolved on native polyacrylamide PhastGels and stained with Coomassie blue.

Vinculin–actin binding assays
Vinculin (in PBS) was incubated at ambient temperature with IpaA-VBS, -VBS2, or -Cterm, and the ability to cosediment with F-actin was assessed as previously described (Bois et al., 2006).

Immunoblot analyses
Levels of IpaA proteins expressed by wild-type and mutant strains of *S. flexneri* were determined using an anti-IpaA–specific antibody (Tran Van Nhieu et al., 1997). Binding of IpaA mutant proteins to vinculin was also assessed in a vinculin overlay assay using I^{125}-labeled vinculin, as previously described (Bourdet-Sicard et al., 1999).

IpaA translocation assays
Levels of IpaA protein translocated inside HeLa cells were assessed as previously described (Kubori and Galán, 2003). Immunoprecipitation was performed using the anti-IpaA2 serum (Tran Van Nhieu et al., 1997). Western blot was performed with anti-IpaA (working dilution 1:10,000) as a primary antibody and protein A-HRP (working dilution 1:10,000; BioRad Laboratories) as a secondary antibody.

Crystallization of the Vh1–IpaA-VBS and –IpaA-VBS2 complexes
Details regarding crystallization of the Vh1–IpaA-VBS and –IpaA-VBS2 complexes can be found in Table S1 and S2, respectively.

X-ray data collection, structure determination, and refinement
Details regarding the collection of x-ray data (Collaborative Computational Project number 4, 1994; Otwinowski and Minor, 1997) and the determination and refinement (Tronrud et al., 1987; Jones et al., 1991; Bricogne, 1997) of the structures of the Vh1–IpaA-VBS and –IpaA-VBS2 complexes are provided in the captions of Table S1 and S2 and S3 and S4, respectively.

Cell culture, *S. flexneri* strains, and bacterial internalization and dissemination assays
HeLa cells were grown in DME supplemented with 10% FCS, Hepes, penicillin, streptomycin, and L-glutamine in 9% CO_2. Caco-2/TC-7 cells were cultured in DME supplemented with 20% FCS and allowed to form polarized monolayers, as previously described (Tran Van Nhieu et al., 2003). Wild-type *S. flexneri* serotype 5 M90T and the *ipaA* mutant were cultured as previously described (Tran Van Nhieu et al., 1997). The *ΔCterm* mutant was generated by cutting pBad:ipaA with *SnaB*I and *Pvu*II, followed by religation to generate a deletion of the last 81 C-terminal residues. The *ΔVBS* mutation was created using the QuickChange II (Stratagene) method using the primer 5′-GACGATACCTCTGCAGAATAACTTACAGATGATATATCTG-3′, which generates a deletion of the last 44 C-terminal residues. The *ΔVBS2* mutation was created using the primers 5′-GATACAATTGATAAAAATCATTCTGCAGAATTACTTA CAGATG-3′ and 5′-CATCTGTAAGTAATTCTGCAGAATGATTTTTATCAATTGTATC-3′ and PCR, which generates a deletion of residues 564–586 of IpaA. Plasmid constructs were subcloned into the vector pCR2.1 (Invitrogen) and transformed into the *ipaA* mutant strain to generate *ipaA/A-ΔCterm*, *ipaA/A-ΔVBS*, and *ipaA/A-ΔVBS2* strains (Fig. S1 A).

Wild-type *S. flexneri*, *ipaA*, *ipaA/A*, *ipaA/A-ΔCterm*, and *ipaA/A-ΔVBS* strains were tested for internalization in HeLa cells using the gentamicin protection assay, as previously described (Perdomo et al., 1994). Bacterial entry and dissemination in polarized Caco-2 cells was determined

as follows. Bacteria grown in exponential phase were resuspended in DME containing 20 mM Hepes, pH 7.3, at a final optical density$_{600nm}$ of 0.06 and used to challenge cell monolayers for 90 min at 37°C. Samples were rinsed and incubated for 6 h in DME containing 10% FCS and 50 mg/ml gentamicin to prevent bacterial extracellular growth and to allow for intercellular dissemination. Samples were fixed and stained for F-actin and LPS, as previously described (Tran Van Nhieu et al., 1997, 2000). Quantification of bacterial invasion and cell–cell spreading in Caco-2 cells monolayers was performed using an epifluorescence microscope (BX50; Olympus). For invasion, the number of infection foci per field was scored with a 20× objective (Olympus) on at least 100 fields in two independent experiments. To assess cell–cell spread of bacteria, the number of infected cells/foci was scored using a 40× immersion objective (Olympus) on at least 30 foci in three independent experiments. Statistical quantification of the surface area and the intensity of vinculin recruitment at *S. flexneri* entry sites was performed from images reconstructed from z stacks corresponding to planes spaced by 0.2 mm, acquired with an epifluorescence microscope (DRMIBe; Leica) equipped with a 63× immersion objective and a piezo (P-721.17, Physik Instrumente), connected to a charge-coupled device camera (CoolSNAP HQ; Princeton Instruments) under the Metamorph software (version 6.3 r1; Universal Imaging Corp.). The plotted data are representative of at least 30 foci in two independent experiments.

The assay used to evaluate cell–cell spreading of wild-type and mutant strains of *S. flexneri* (Tran Van Nhieu et al., 2003) was derived from the plaque assay that has been extensively used to assess *S. flexneri* dissemination (Oaks et al., 1985). Translocation and immunofluorescence assays to determine levels of intracellular IpaA proteins and vinculin localization were performed as previously described (Tran Van Nhieu et al., 1997).

Accession codes

The atomic coordinates of the Vh1–IpaA-VBS and Vh1–IpaA-VBS2 crystal structures have been deposited in the Protein Data Bank under accession codes 2GWW and 2HSQ, respectively.

Online supplemental material

Fig. S1 shows a schematic of the various IpaA and vinculin constructs used in this study. Fig. S2 shows a stereo view of Tyr-613 of IpaA-VBS and Tyr-567 of IpaA-VBS superimposed onto Ile-1950, as seen in the vinculin–talin-VBS3 crystal structure (Izard et al., 2004), as well as details of the interaction of Lys-569 or Ala-615 of IpaA with Leu-54 and Val-57 of vinculin. Tables S1–S4 show the data reduction and crystallographic refinement statistics for the Vh1–IpaA-VBS and–IpaA–VBS2 structures. Online supplemental material is available at http://www.jcb.org/cgi/content/full/jcb.200605091/DC1.

We are indebted to J.L. Cleveland (St. Jude Children's Research Hospital, Memphis, TN; SJ) for helpful discussions and for critical review of the manuscript; G. Bricogne and C. Vonrhein (Global Phasing, Ltd., Cambridge, UK; GPhL) for continuous advice and making autoBUSTER available for crystallographic refinement; D. Myzka (University of Utah, Salt Lake City, UT) for SPR; our in-house Hartwell Center for peptide synthesis; the Hauptman-Woodward Institute for determining the initial crystallization conditions; C.R. Ross (SJ) for maintaining the computing facilities; M.M. Ellis, V.K. Morris, Christen Gergory (all from SJ), and M. Roberts (GPhL) for technical assistance; and the 19ID and 22ID staff at the Advanced Photon Source for synchrotron support. Some of this work was carried out in M. Giovannini's laboratory (Centre d'Etude du Polymorphisme Humain).

This work was supported by grants from the National Institutes of Health (AI067949 and GM071596 to T. Izard), a Cancer Center Support grant (CA21765), and by the American Lebanese Syrian Associated Charities.

Submitted: 15 May 2006
Accepted: 5 October 2006

Note added in proof. While our article was under review, Hamiaux et al. (Hamiaux, C. van Eerde, C. Parsot, J. Broos, and B.W. Dijkstra. 2006. *EMBO Reports*. 7:794–799) reported that the C-terminal domain of IpaA (residues 560–633) was capable of binding to vinculin's Vh1 domain in a 2:1 stoichiometry. Our findings that the binding of IpaA-VBS and IpaA-VBS2 to the Vh1 domain is mutually exclusive suggests that the IpaA may be able to simultaneously bind to two molecules of vinculin.

References

Bakolitsa, C., D.M. Cohen, L.A. Bankston, A.A. Bobkov, G.W. Cadwell, L. Jennings, D.R. Critchley, S.W. Craig, and R.C. Liddington. 2004. Structural basis for vinculin activation at sites of cell adhesion. *Nature*. 430:583–586.

Bakolitsa, C., J.M. de Pereda, C.R. Bagshaw, D.R. Critchley, and R.C. Liddington. 1999. Crystal structure of the vinculin tail suggests a pathway for activation. *Cell*. 99:603–613.

Bois, P.R.J., R.A. Borgon, C. Vonrhein, and T. Izard. 2005. Structural dynamics of α-actinin-vinculin interactions. *Mol. Cell. Biol.* 25:6112–6122.

Bois, P.R.J., B.P. O'Hara, D. Nietlispach, J. Kirkpatrick, and T. Izard. 2006. The vinculin binding sites of talin and α-actinin are sufficient to activate vinculin. *J. Biol. Chem.* 281:7228–7236.

Borgon, R.A., C. Vonrhein, G. Bricogne, P.R.J. Bois, and T. Izard. 2004. Crystal structure of human vinculin. *Structure*. 12:1189–1197.

Bourdet-Sicard, R., C. Egile, P.J. Sansonetti, and G. Tran Van Nhieu. 1999. Binding of the *Shigella* protein IpaA to vinculin induces F-actin depolymerization. *EMBO J.* 18:5853–5862.

Bricogne, G. 1997. The Bayesian viewpoint in crystallography: basic concepts and applications. *Methods Enzymol.* 276:361–423.

Chandrasekar, I., T.E. Stradal, M.R. Holt, F. Entschladen, B.M. Jockusch, and W.H. Ziegler. 2005. Vinculin acts as a sensor in lipid regulation of adhesion-site turnover. *J. Cell Sci.* 118:1461–1472.

Chen, H., D.M. Cohen, D.M. Choudhury, N. Kioka, and S.W. Craig. 2005. Spatial distribution and functional significance of activated vinculin in living cells. *J. Cell Biol.* 169:459–470.

Cohen, D.M., H. Chen, R.P. Johnson, B. Choudhury, and S.W. Craig. 2005. Two distinct head-tail interfaces cooperate to suppress activation of vinculin by talin. *J. Biol. Chem.* 280:17109–17117.

Collaborative Computational Project Number 4. 1994. The CCP4 suite: programs for protein crystallography. *Acta Cryst.* D50:760–763.

Critchley, D.R. 2004. Cytoskeletal proteins talin and vinculin in integrin-mediated adhesion. *Biochem. Soc. Trans.* 32:831–836.

Fillingham, I., A.R. Gingras, E. Papagrigoriou, B. Patel, J. Emsley, D.R. Critchley, G.C. Roberts, and I.L. Barsukov. 2005. A vinculin binding domain from the talin rod unfolds to form a complex with the vinculin head. *Structure*. 13:65–74.

Galkin, V.E., A. Orlova, M.S. VanLoock, D. Zhou, J.E. Galán, and E.H. Egelman. 2002. The bacterial protein SipA polymerizes G-actin and mimics muscle nebulin. *Nat. Struct. Biol.* 9:518–521.

Gilmore, A.P., and K. Burridge. 1996. Regulation of vinculin binding to talin and actin by phosphatidyl-inositol-4-5-bisphosphate. *Nature*. 381:531–535.

Gouin, E., M.D. Welch, and P. Cossart. 2005. Actin-based motility of intracellular pathogens. *Curr. Opin. Microbiol.* 8:35–45.

Isberg, R.R., and S. Falkow. 1985. A single genetic locus encoded by *Yersinia pseudotuberculosis* permits invasion of cultured animal cells by *Escherichia coli K-12*. *Nature*. 317:262–264.

Izard, T., G. Evans, R.A. Borgon, C.L. Rush, G. Bricogne, and P.R. Bois. 2004. Vinculin activation by talin through helical bundle conversion. *Nature*. 427:171–175.

Izard, T., and C. Vonrhein. 2004. Structural basis for amplifying vinculin activation by talin. *J. Biol. Chem.* 279:27667–27678.

Johnson, R.P., and S.W. Craig. 1995. F-actin binding site masked by the intramolecular association of vinculin head and tail domains. *Nature*. 373:261–264.

Jones, T.A., J.-Y. Zou, S.W. Cowan, and M. Kjeldgaard. 1991. Improved methods for building protein models in electron density maps and the location of errors in these models. *Acta. Crystallogr. A*. 47:110–119.

Kubori, T., and J.E. Galán. 2003. Temporal regulation of salmonella virulence effector function by proteasome-dependent protein degradation. *Cell*. 115:333–342.

Lilic, M., V.E. Galkin, A. Orlova, M.S. VanLoock, E.H. Egelman, and C.E. Stebbins. 2003. *Salmonella* SipA polymerizes actin by stapling filaments with nonglobular protein arms. *Science*. 301:1918–1921.

Loisel, T.P., R. Boujemaa, D. Pantaloni, and M.F. Carlier. 1999. Reconstitution of actin-based motility of *Listeria* and *Shigella* using pure proteins. *Nature*. 401:613–636.

McGhie, E.J., R.D. Howard, and V. Koronakis. 2004. Control of actin turnover by a *Salmonella* invasion protein. *Mol. Cell*. 13:497–510.

Niyogi, S.K. 2005. Shigellosis. *J. Microbiol.* 43:133–143.

Otwinowski, Z., and W. Minor. 1997. Processing of X-ray diffraction data collected in oscillation mode. *Methods Enzymol.* 276:307–326.

Oaks, E.V., M.E. Wingfield, and S.B. Formal. 1985. Plaque formation by virulent *Shigella flexneri*. *Infect. Immun.* 48:124–129.

Perdomo, O.J., J.M. Cavaillon, M. Huerre, H. Ohayon, P. Gounon, and P.J. Sansonetti. 1994. Acute inflammation causes epithelial invasion and mucosal destruction in experimental shigellosis. *J. Exp. Med.* 180:1307–1319.

Stebbins, C.E., and J.E. Galán. 2001. Structural mimicry in bacterial virulence. *Nature*. 412:701–705.

Tran Van Nhieu, G., A. Ben-Ze'ev, and P.J. Sansonetti. 1997. Modulation of bacterial entry into epithelial cells by association between vinculin and the *Shigella* IpaA invasin. *EMBO J.* 16:2717–2729.

Tran Van Nhieu, G., R. Bourdet-Sicard, G. Dumenil, A. Blocker, and P.J. Sansonetti. 2000. Bacterial signals and cell responses during *Shigella* entry into epithelial cells. *Cell. Microbiol.* 2:187–193.

Tran Van Nhieu, G., C. Clair, R. Bruzzone, M. Mesnil, P. Sansonetti, and L. Combettes. 2003. Connexin-dependent intercellular signaling increases *Shigella* invasion and dissemination in epithelial cells. *Nat. Cell Biol.* 5:720–726.

Tronrud, D.E., L.F.T. Eyck, and B.W. Matthews. 1987. An efficient general-purpose least-squares refinement program for macromolecular structures. *Acta Crystallogr.* A43:489–501.

Zhou, D., M.S. Mooseker, and J.E. Galán. 1999. Role of the *S. typhimurium* actin-binding protein SipA in bacterial internalization. *Science*. 283:2092–2095.